Bulletin of Volcanology (2019) 81:30
https://doi.org/10.1007/s00445-019-1289-6

RESEARCH ARTICLE

Surface crusting of volcanic ash deposits under simulated rainfall

Inga Tarasenko[1] · Charles L. Bielders[1] · Alicia Guevara[2] · Pierre Delmelle[1]

Received: 22 October 2018 / Accepted: 15 March 2019

Abstract

Explosive volcanic eruptions can have severe impacts on watershed hydrology. Among them, surface crusting of volcanic ash fallout following rainfall has been shown to favour runoff, erosion and lahar initiation. It may also hamper seed emergence and depress plant growth. However, ash crust formation is poorly understood. Reconstructed ash deposits were subjected to simulated rainfall to investigate the microscale morphological modifications of the ash deposit surface in response to raindrop impact. Ash samples from three volcanic eruptions (Mt. Merapi, MER, Indonesia; Eyjafjallajökull, EYJA, Iceland; and San Cristobal, SC, Nicaragua) with different particle size distributions and soluble salt contents were used in the experiment. Microcraters and micropeaks formed on the surface of all ash deposits after rainfall initiation. This was accompanied by fine material (also referred to as micromass) accumulation in the form of one or several layers, a few tens to hundreds of micrometres thick. Such morphological changes point to structural crust formation. The crusts consisted of a thin layer of tightly packed clay and silt-size ash particles (SC), overlain by loose coarser materials in micro-craters (MER) or by an almost continuous coarse-grained layer (EYJA). In all cases, the surface crust had a reduced porosity compared with the bulk material. Depending on ash particle size, crusting was governed by splash, compaction and vertical sorting (MER), vertical particle sorting (EYJA) or compaction (SC). No samples showed evidence of particle cementation through secondary salt precipitation. Our results shed new light on the mechanisms responsible for post-depositional crusting of a natural ash deposit.

Keywords Volcanic ash · Ash deposit · Structural crust · Lahar initiation · Rainfall simulation

Introduction

The deposition of volcanic ash produced by explosive eruptions induces various effects on terrestrial environments (Cook et al. 1981; Dale et al. 2005; Ayris and Delmelle 2012; Arnalds 2013). An ash layer on soil may modify surface albedo and consequently, soil temperature and water balance (Cook et al. 1981; Black and Mack 1986; Jones et al. 2007). An ash deposit that is less porous and hydraulically conductive than the underlying bulk soil also leads to water transport limitations. Thus, ash on soil can reduce water infiltration and storage, thereby increasing the risk of runoff and lahar initiation (e.g. Nammah et al. 1986; Hendrayanto et al. 1995; Pierson and Major 2014). Importantly, this effect is enhanced by surface sealing/crusting of the ash deposit (Leavesley et al. 1989; Craig et al. 2016; Jones et al. 2017). In soil science, a surface crust is defined as a thin layer of consolidated material at the immediate soil surface with significantly different structural and mechanical characteristics than the underlying bulk soil (Mualem et al. 1990; Assouline 2004). A soil crust (or seal when wet) develops in response to temporal and spatial interactions between physical, biological and chemical properties and processes (e.g. Mualem et al. 1990; Assouline 2004; Baumhardt and Schwartz 2004).

Post-deposition hardening of fine-textured ash deposits to produce a surface crust after wetting has long been reported; it has been held responsible for the impairment of emerging crop seedlings and diminished plant growth (e.g. Segerstrom 1950; Waldron 1967; Antos and Zobel 2005; Arnalds 2013).

Editorial responsibility: P-S. Ross

Electronic supplementary material The online version of this article (https://doi.org/10.1007/s00445-019-1289-6) contains supplementary material, which is available to authorized users.

✉ Inga Tarasenko
inga_t7@hotmail.com

[1] Environmental Sciences, Earth and Life Institute, UCLouvain, Croix du sud 2, bte L7.05.02, 1348 Louvain-la-Neuve, Belgium

[2] Departamento de Metalurgia Extractiva, Escuela Politécnica Nacional, Quito, Ecuador

Published online: 13 April 2019

Manville et al. (2000) pointed to a relationship between surface sealing/crusting of fine-grained ash and lahar frequencies at Ruapehu volcano, New Zealand. A similar conclusion was reached in a study conducted at Unzen volcano, Japan (Yamakoshi and Suwa 2000). While there is compelling evidence that the surface of a newly emplaced ash deposit is susceptible to crusting, the crust formation mechanisms are poorly understood. At Parícutin volcano, Mexico, Segerstrom (1950) posited that surface crusting of ash deposits emplaced by the 1943 eruption was largely the result of compaction and sorting of the ash particles by raindrop impact and erosion. In contrast, Waldron (1967) argued that the continued formation of a surface crust in ash deposited during the 1963–1965 eruption of Irazú volcano, Costa Rica, was primarily due to evaporation-driven precipitation of halide salts (originally dissolved from the ash surfaces) within the deposit porosity. At Kilauea volcano, Hawaii, hardening of the surface of a basaltic tephra deposit in the Kau Desert was attributed to weathering reactions promoted by volcanogenic acid depositions (Malin et al. 1983).

There is a plethora of experimental and theoretical investigations that examine the processes and factors governing soil crust development (e.g. Mualem et al. 1990; Valentin and Bresson 1992; Bresson and Valentin 1993; Assouline 2004; Armenise et al. 2018). However, no equivalent effort has been made to describe surface crusting of volcanic ash deposits. Here, we report the results of a laboratory experiment aimed at shedding light on the mechanisms involved in ash crust formation. Three laboratory-reconstructed ash deposits of contrasting texture and soluble salt content were subjected to simulated rainfall of constant intensity and kinetic energy but different durations. We document the microscale morphological modifications of the surface of the ash deposits, and we infer the main mechanisms responsible for crust formation.

Materials and methods

Experiment configuration

Ash material

Three ash samples collected fresh (i.e. prior to exposure to rain or snow) from different volcanoes were tested (Table 1). The ash materials correspond to the 2010 eruptions of Mt. Merapi (MER, Indonesia) and Eyjafjallajökull (EYJA, Iceland) and the 2000 eruption of San Cristobal (SC, Nicaragua). The particle size distributions of the three ash specimens measured by laser particle size analysis (COULTER LS 100Q) are shown in Table S1 in the supplementary material. EYJA is the coarsest ash ($D_{50} = 76.4$ µm; mean 182.43 µm), whereas MER is the finest ($D_{50} = 29.7$ µm; mean 51.15 µm). SC is coarser than MER ($D_{50} = 38.9$ µm; mean 76.31 µm). The three ash samples also differ in their leachate compositions (Table S2). The total dissolved solids (TDS) content of SC is ~ 13 and ~ 32 times higher than that of MER and of EYJA, respectively. Together, calcium and sulphate account for ~ 93% of SC's TDS.

Laboratory-reconstructed ash deposit

The ash deposits were reconstructed in the laboratory by modifying a protocol developed earlier for studying soil crusting (Bielders and Grymonprez 2010). To be able to assess morphological changes in the ash deposit following exposure to simulated rainfall, it was important to produce a homogeneous deposit to avoid particle sorting during its reconstruction (supplementary material, Fig. S1a, b). Previous works on crusting for a wide range of soil textures indicate that the formation of a surface structural crust is typically restricted to the upper few millimetres (e.g. Mualem et al. 1990; Valentin and Bresson 1992; Bielders and Baveye 1995a, b). Therefore, a 2-cm thick deposit was considered adequate for studying surface crust formation.

Rainfall simulator

The laboratory reconstructed ash deposits were exposed to various amounts of rainfall using a simulator (supplementary material, Fig. S1c). The experiment was conducted under near-constant, relatively low rainfall intensities, i.e. 9.0 ± 0.3, 10.3 ± 0.8 and 9.4 ± 0.4 mm h^{-1} for MER, SC and EYJA, respectively, in order to avoid water ponding. The presence of ponded water would create unrealistic surface conditions in the experimental columns since in most natural conditions, ponded water flows away laterally. Further, we sought to characterise the first

Table 1 Brief description of the three ash samples used in the study

Sample code	Volcano	Eruption date	Eruption style	Composition	Reference
MER	Merapi	26.10.2010	Magmatic/dome explosion	Andesite	a
SC	San-Cristobal	22.01.2000	Phreatic/strombolian	Basaltic andesite	b
EYJA	Eyjafjallajökull	23.04.2010	Phreatomagmatic	Trachyandesite	c

a, Damby et al. (2013); b, Global Volcanism Program (2000); c, Sigmarsson et al. (2011)

stage of structural crust development, which takes place in the absence of ponded water (Valentin and Bresson 1992). The temporal evolution of surface crusting was assessed by exposing the ash deposits to 5, 10, 15 and 20 mm of rainfall.

In order to verify that changes in the characteristics of the ash deposit exposed to rain resulted from raindrop impact-related processes, a set of samples was covered with a pre-wetted, highly permeable and low water retention capacity Scotch Brite™ sponge during rainfall simulation. The sponge absorbs the kinetic energy of the falling drops but does not hamper water infiltration. Each combination of ash type ($n = 3$), rainfall amount ($n = 4$) and wetting method ($n = 2$) was replicated three times.

Post-experiment analyses

Sample preparation

Following rainfall application, the ash deposits were left overnight to allow water to drain. They were subsequently dried at 55 °C for 72 h before impregnation with an epoxy resin (EBL 1466™) under vacuum and at room temperature. The resin-embedded samples were cut vertically. One-half was impregnated a second time with high quality, transparent resin (Epoxicure 2™). Thin sections were prepared from slabs cut from the consolidated material and analysed by optical microscopy. The other half of the resin-embedded samples was used to make polished sections.

The polished sections were examined by optical microscopy at magnifications of × 7 and × 16 prior to selecting representative sample areas for scanning electron microscope (SEM) analysis. The corresponding polished sections were cleaned in an ultrasonic bath and coated with gold prior to the SEM measurements (Tescan-Vega© instrument). Backscattered electron micrographs were obtained at 25 kV.

Micromorphological analysis

A cross-sectional image of each ash deposit was obtained by stitching the SEM images together (Fiji© software, https://fiji.sc). Depending on magnification settings on the SEM, the pixel size was 0.48 or 1.28 μm (MER and SC), and 0.7 or 1.89 μm (EYJA). Grain-size distributions in the deposits affected by raindrop impact were estimated by measuring the long axis of 40 particles (see the supplementary material for details). Three-level greyscale images, generated through image analysis, were used to derive porosity estimates (see the supplementary material for details).

Microtopography analysis

The microtopography of the ash deposit surface subjected to rainfall was described in terms of spacing and amplitude of surface features (micro-peaks and micro-craters) (Fig. S2). micropeak and microcrater counts (P_c and C_c in #peaks or #craters cm^{-1}, respectively) were determined from photos of the deposit surfaces (Fig. 1). The evaluation length used was typically 4 cm, i.e. the edges of the deposit surface were excluded. A surface roughness index (R_{cp}) was calculated as the average apparent vertical distance between a microcrater and its neighbouring micropeaks (i.e. microcrater depth, Fig. S2). An average R_{cp} value was obtained for each sample from the analysis of a portion (~ 4 cm in length) of the thin section.

Statistics

The porosity values of bulk and near-surface layers were compared by means of a paired t test, with a p value of 0.05. A one-way analysis of variance (ANOVA1) in combination with a Tukey's test ($p < 0.05$) was performed to test C_c, P_c and R_{cp} for significant differences across rainfall amounts (i.e. 5, 10, 15 and 20 mm).

Results

Visually, only the ash deposits subjected to direct raindrop impact showed signs of particle rearrangement. In contrast, cross-sectional SEM images of the rain-protected MER, SC and EYJA deposits did not show any signs of particle reorganisation in the vicinity of the deposit surface (Fig. S3). Below, we focus specifically on these drop-impacted samples, for which surface microtopography and morphological measurements are displayed in Figs. 1, 2, 3, 4, 5, 6, 7 and 8 and compiled in Table S3.

Microtopography

MER ash deposit

The surface of MER ash deposit changed immediately after the onset of rainfall (Fig. 1a). Ash pellets formed rapidly, but these structures were transitory as they disappeared when the surface became moist and riddled with micropeaks and microcraters. After 5 mm of rainfall, P_c and C_c were on average 2.1 ± 0.2 and 2.0 ± 0.2 cm^{-1}, respectively (Fig. 2a). Parameters P_c and C_c decreased by more than 40% at higher cumulative rainfall values. At this point, the ash surface became "shiny", suggesting gradual water saturation (pre-ponding stage). After 20 mm of rainfall, P_c and C_c were less than 1 cm^{-1}. A surface roughness index (R_{cp}) increased from

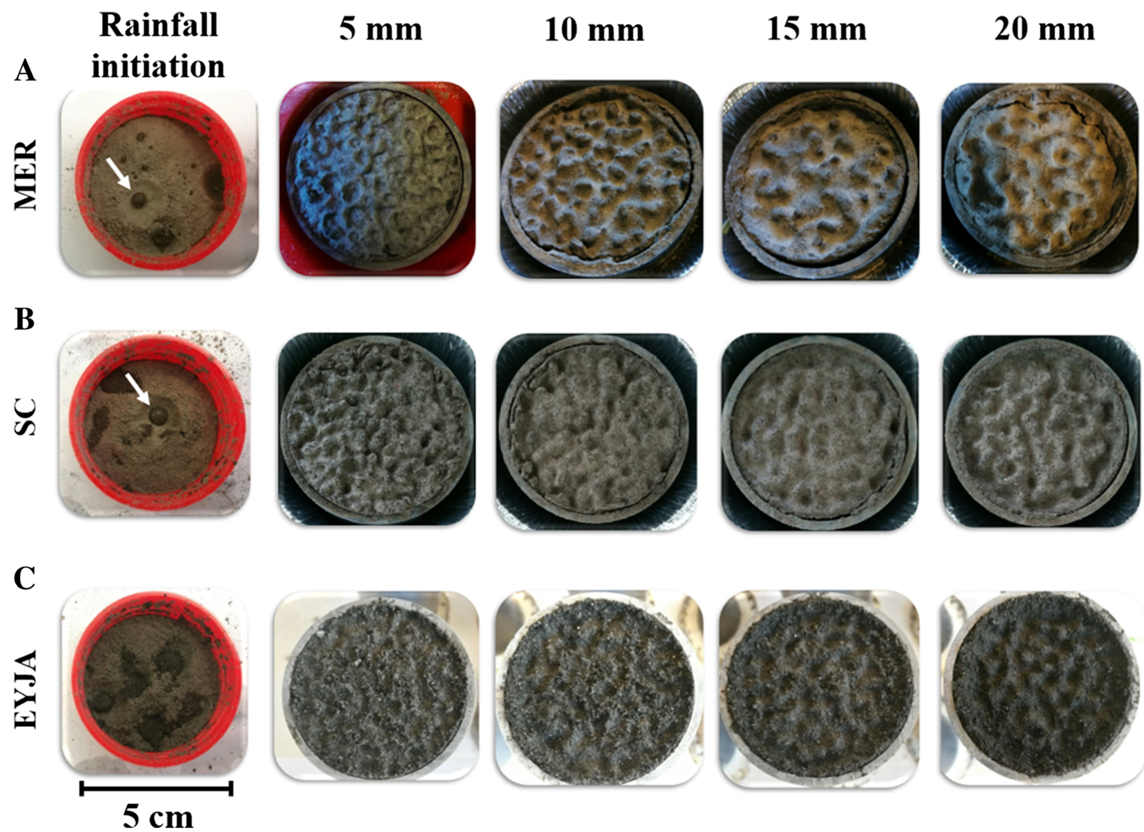

Fig. 1 Photographs of the surface of MER (**a**), SC (**b**) and EYJA (**c**) ash deposits after exposure to 5, 10, 15 and 20 mm of simulated rainfall. White arrows point to ash pellets formed on the deposit surface immediately after rainfall initiation

1.3 ± 0.1 mm (5 mm of rainfall) to 1.9 ± 0.1 mm (10 mm of rainfall), and then slightly decreased to 1.6 ± 0.2 mm after 20 mm of rainfall (Fig. 2a). Water ponding did not occur.

SC ash deposit

Similar to MER, transient ash pellet formation occurred at the surface of SC deposit as soon as rain started (Fig. 1b). Five millimetres of rainfall resulted in riddling of the surface with micropeaks and microcraters ($P_c = 2.0 \pm 0.1$ cm^{-1}, $C_c = 1.7 \pm 0.2$ cm^{-1}; Fig. 2b). Parameter P_c decreased significantly after 15 mm of rainfall and was close to 1 cm^{-1} at the end of the experiment. Parameter C_c decreased slightly from 1.6 ± 0.1 cm^{-1} (10 mm of rain) to 1.0 ± 0.2 cm^{-1} (20 mm of rain). Water infiltration through the deposit became more limited after 15 mm of rainfall, although ponding did not occur. In contrast to MER, R_{cp} significantly increased from 1.5 ± 0.1 mm (5 mm of rainfall) to 2.1 ± 0.2 mm (20 mm of rainfall; Fig. 2b).

EYJA ash deposit

Pellet formation was minimal for EYJA, and micropeaks and microcraters were only weakly visible on the deposit surface after 5 mm of rainfall (Fig. 1c). With additional rainfall, micropeaks and microcraters developed more strongly. However, P_c, C_c and R_{cp} did not change significantly between 10 and 20 mm of rainfall (Fig. 2c). There were no visible signs of decreased water infiltration during the experiment.

Micromorphology

MER ash deposit

The thin sections and SEM images clearly highlighted particle reorganisation near the surface of the MER deposit. After 5 mm of rainfall, this manifested as a thin (~ 70–80 μm) layer comprised of closely packed fine ash particles extending laterally across the deposit surface, although mostly in microcraters (Fig. 3a). Occasionally, coarser particles (thickness ~ 120 μm) were observed at the surface in microcraters. The SEM images indicated that the thin layer consisted predominantly of silt- and clay-size particles (Fig. 4a). It further developed after 10 mm of rainfall (Fig. 3b). In microcraters, coarser material (fine and very fine sand) continued to accumulate on top of the thin layer (Fig. 4b). With additional rainfall, multi-layered structures appeared, again more prominently in microcraters (Fig. 3c). It consisted of silt- and clay-size material (i.e. micromass) alternating with sand-size materials. The

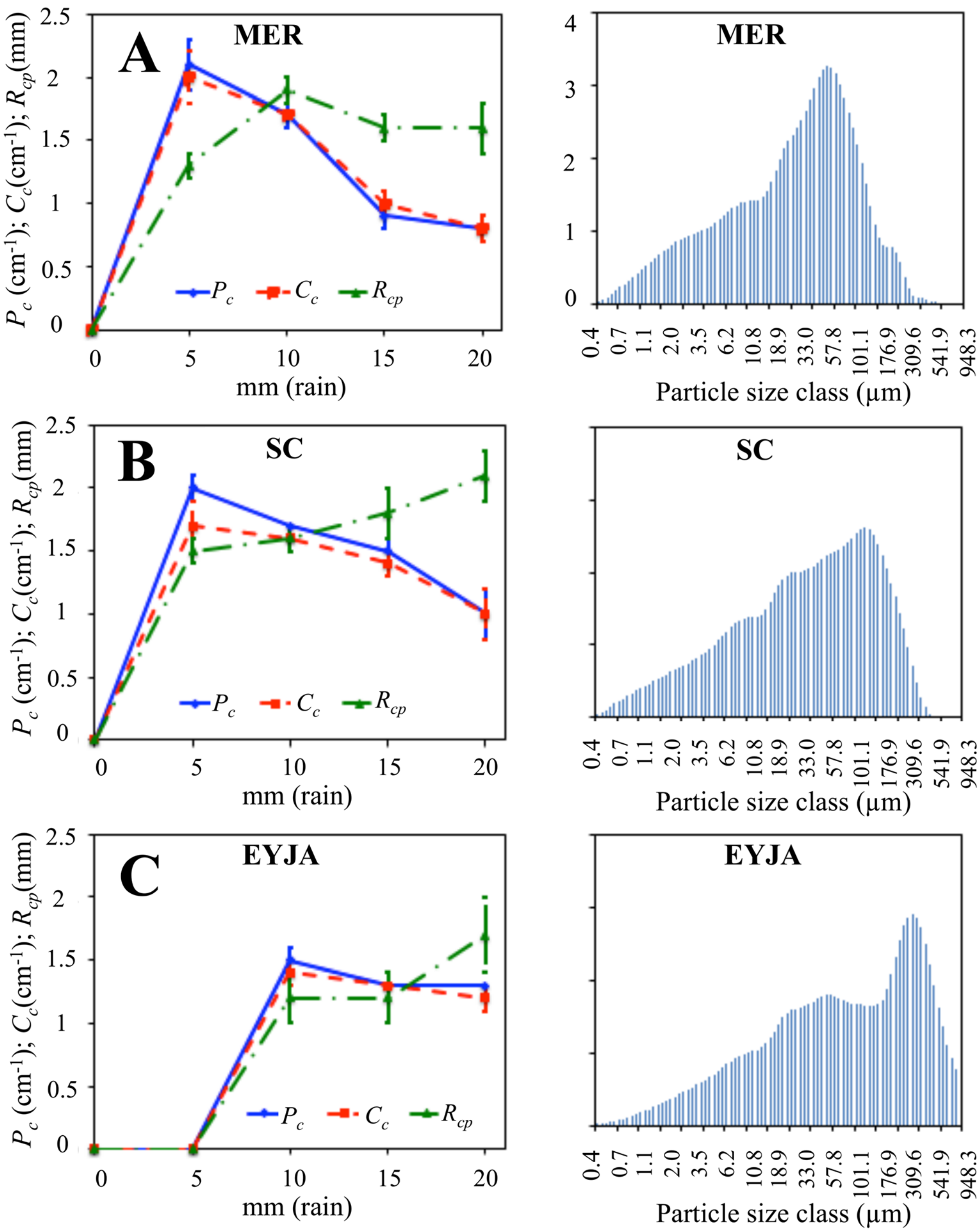

Fig. 2 Micropeak (P_c in #peaks cm^{-1}) and microcrater (C_c in #craters cm^{-1}) counts, surface roughness index (R_{cp}) and bulk particle size distribution as determined by laser diffraction analysis of the MER (**a**), SC (**b**) and EYJA (**c**) ash deposits prior to simulated rainfall. P_c, C_c and R_{cp} are the means of three sample replicates. Error bars represent standard errors from the means

multi-layered structures continued to develop until the end of the rainfall simulation (Figs. 3d, e and 4c), by which time, they had a total thickness of up to ~1.26 mm (Table S3). In parallel, more coarse particles accumulated at the surface of the ash deposit. Careful examination of the SEM images did not provide evidence for chemical cementation of ash particles near the deposit surface.

SC ash deposit

Similar to MER, application of 5 mm of rainfall to SC ash deposit led to particle reorganisation and appearance of a thin (~40–50 µm) layer of tightly packed clay-size particles, more prominently in microcraters (Figs. 5a and 6a). The thin layer became mostly laterally continuous at higher cumulative rainfall amounts, although some micropeaks remained unaffected (Fig. 5b–e). After 10 and 15 mm of rainfall, the thin layer was dominated by clay- and fine to coarse silt-size particles (Fig. 6b, c and d). Independent of the rainfall amount, coarser particles occurred occasionally in microcraters and micropeaks on top of the thin layer. Analysis of the SEM images indicated that the coarse material was dominated by very fine sand-, fine silt- and coarse silt-size particles. At the end of

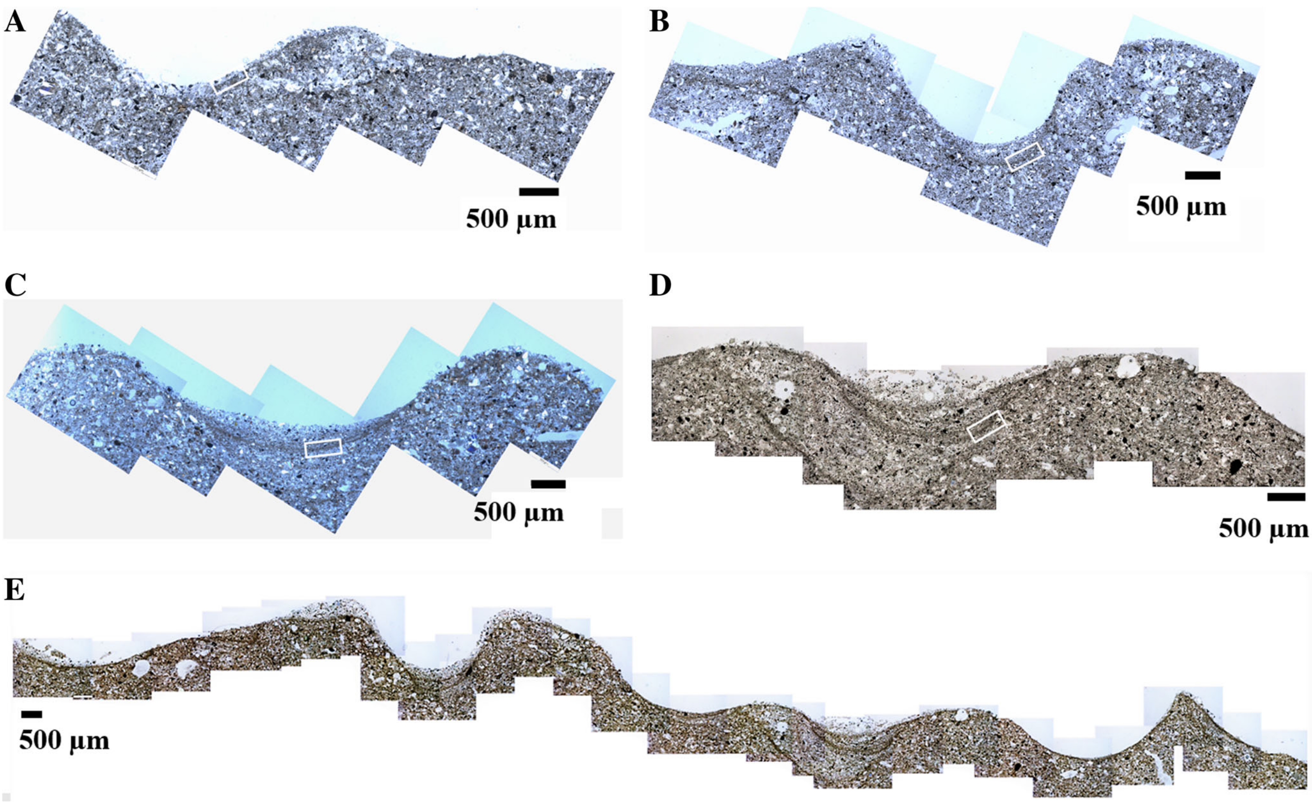

Fig. 3 Optical microscope images (stitched) of the thin cross sections of the MER ash deposit after exposure to 5 mm (**a**), 10 mm (**b**), 15 mm (**c**) and 20 mm (**d**) of simulated rainfall. The rectangle outlined in white highlights the location of the thin layer comprised of tightly packed ash particles. The full cross-section of the ash deposit surface exposed to 20 mm of simulated rain is shown in (**e**)

the rainfall simulation, the total thickness of the deposit affected by particle reorganisation was ~ 120 µm when the layer of coarse particles was absent; it nearly doubled when it was present (Table S3). Particle reorganisation did not occur in the bulk material beneath the surface (Fig. 6e), and secondary chemical precipitates were not detected near the deposit surface.

EYJA ash deposit

Although more erratically than in MER and SC, the thin sections and SEM images also highlighted particle reorganisation near the surface of EYJA deposit (Fig. 7a–e, Fig. 8a–c) compared with the bulk layer unaffected by drop impact (Fig. 8d). Again, cementation of ash particles in the rain-treated deposits did not occur. Analysis of the thin sections and SEM images of the samples exposed to 20 mm of rainfall revealed loose accumulations of fine to coarse sand-size particles at the surface, forming a ~ 820 µm thick band (Table S3). A discontinuous, ~ 230 µm-thick layer made of tightly packed clay-, fine silt-, coarse silt- and very fine sand-size particles was observed immediately below the coarser material accumulation. At lower cumulative rainfall amounts, the formation of the thin layer of tightly packed particles was less clear (Fig. 7a–c) and was confirmed only in microcraters (Fig. 8a–c). In contrast to MER and SC, the thickness of the deposit affected by particle reorganisation did not vary with cumulative rainfall (Table S3).

Porosity measurements

The thin layer of closely packed silt- and clay-size ash particles, which formed near the surface of the MER deposit upon exposure to rainfall, showed a reduced porosity (by up to 17%) compared with that of the subsurface bulk material (Fig. 9; Table S4). The difference was statistically significant ($p < 0.05$), irrespective of rainfall amount. In contrast, a comparatively higher (~ 10%) porosity was measured for the coarser material found on top of the thin layer.

Similar to MER, the porosity of the dense thin layer near the surface of the SC sample exposed to 5, 10, 15 and 20 mm of rainfall was lower (by up to 16%) than that measured for the bulk part of the ash deposit (Fig. 10; Table S4).

Compared with the porosity of the bulk deposit material, the porosity of the thin layer was lower by up to 23% after 10 to 20 mm of rainfall. In contrast, the layer of coarser particles (identified at 10 and 15 mm rainfall) above the thin layer

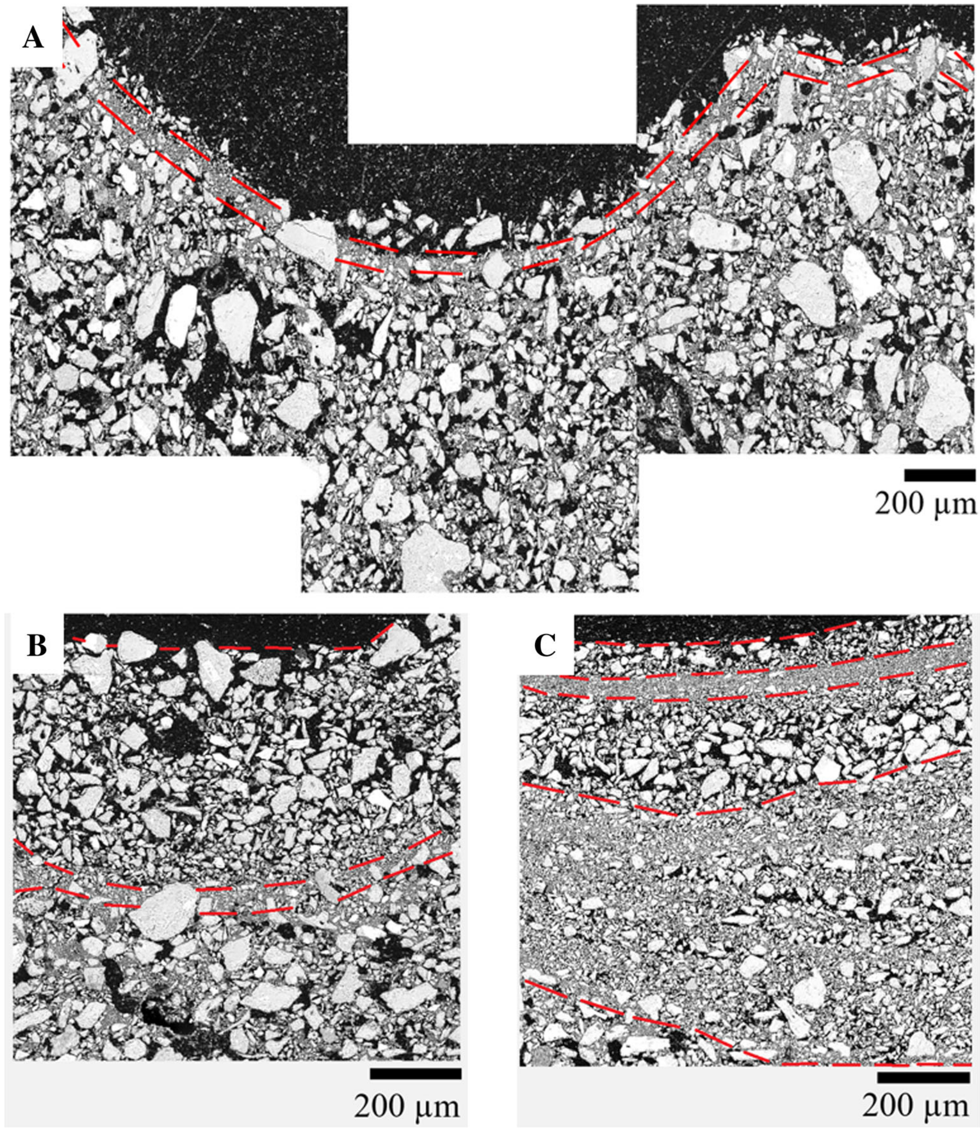

Fig. 4 SEM images of polished cross sections of the MER ash deposit after exposure to 5 (**a**), 10 (**b**) and 20 mm (**c**) of simulated rainfall. The red dashed lines in (**a**), (**b**) and (**c**) delineate the near-surface layer within microcraters where particle reorganisation took place. The bulk material under this layer was unaffected by raindrop impact

exhibited 8–22% higher porosity than that of the bulk ash deposit (Fig. 11; Table S4).

Discussion

Changes in the microtopography of the ash deposit surface

Raindrops impacting the dry surfaces of MER and SC ash deposits caused the transient formation of pellets (Fig. 1a and b). Similarly, Jones et al. (2017) reported rapid, but short-lived, appearance of pellets at the surface of an ash bed subjected to simulated rainfall. By analogy with soils subjected to rainfall (McHale et al. 2005), ash pellet formation may relate to particle hydrophobicity. With the increasing addition of rainwater, the ash became more hydrophilic, impeding further pellet development. The process stopped as the entire ash deposit surface wetted up. The hydrophobicity of volcanic ash is poorly documented. Li et al. (1997) argued that hydrophobic ash is generated by eruptions with a dominantly magmatic fragmentation mechanism, whereas hydrophilic ash is preferentially associated with eruptions with a strong phreatomagmatic component (i.e. involving magma-water interaction). MER ash belongs to the former style of eruption, whereas EYJA ash was collected during the phreatomagmatic phase of the 2010 eruption of Eyjafjallajölull (i.e. phase I according to Gudmundsson et al. 2012). The case of SC is less clear as this ash, which contains hydrothermal minerals (Delmelle et al. 2005), may have been emitted as a result of phreatic and strombolian explosions (Global Volcanism Program 2000). Ash pellets did not occur upon wetting of EYJA

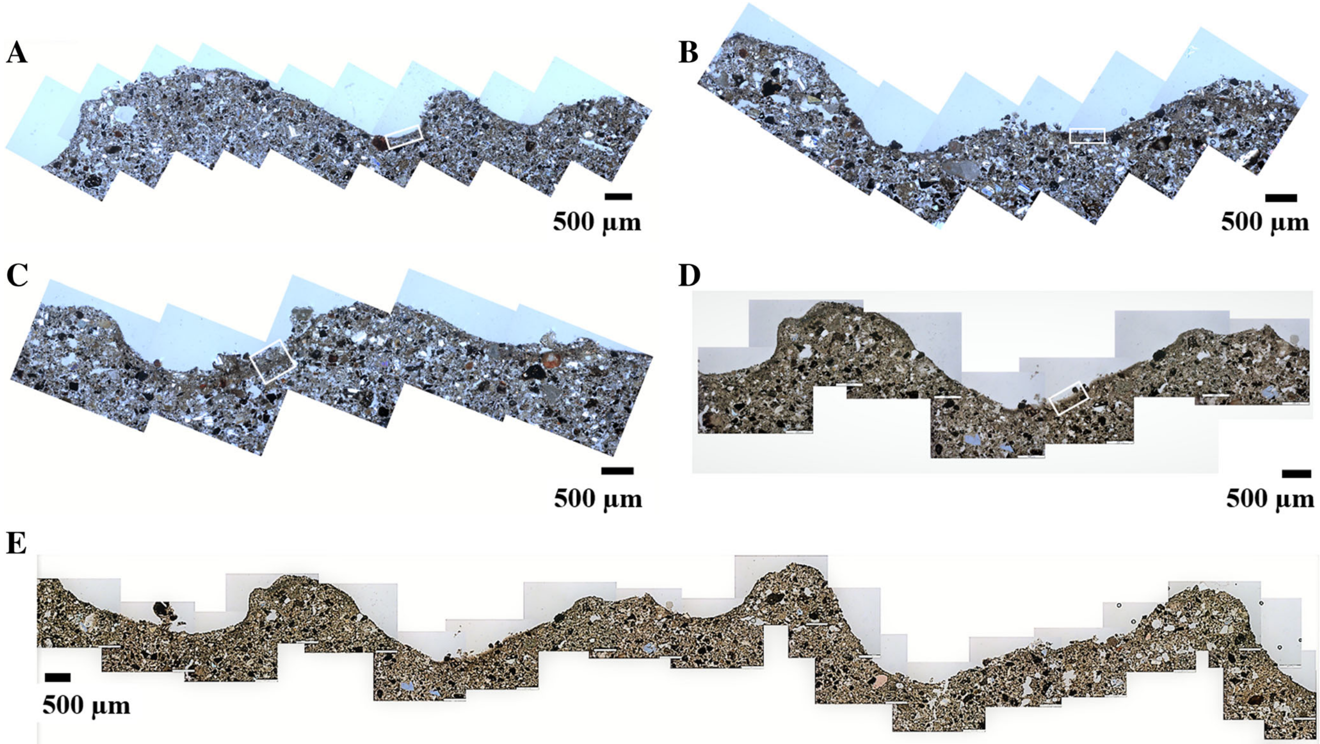

Fig. 5 Optical microscope images (stitched) of the thin cross sections of the SC ash deposit after exposure to 5 mm (**a**), 10 mm (**b**), 15 mm (**c**) and 20 mm (**d**) of simulated rainfall. The rectangle outlined in white indicates the thin layer of tightly packed ash particles. The full cross section of the ash deposit surface exposed to 20 mm of simulated rain is shown in (**e**)

deposit (Fig. 1c), possibly reinforcing the idea that hydrophobicity plays an important role in their formation. Alternatively, the coarser texture of EYJA ash (Table S1 and Fig. 2) may have facilitated water penetration as raindrops hit the deposit surface, thereby preventing pellet development.

Raindrop impacts led to the formation of microcraters and micropeaks at the surface of the ash deposit after 5 mm (MER and SC) and 10 mm (EYJA) of cumulative rainfall. Parameters C_c and P_c tended to decrease with cumulative rainfall applied to MER and SC (Fig. 2a and b), revealing an increase in micropeak and microcrater width over time. This may have resulted from a change in the mechanical properties of the ash material, which, upon gradual saturation of the deposit, increasingly behaved as a rigid layer when falling raindrops impinged on the surface (Moss 1991). A more rigid surface tends to decrease the angle formed by the surface and the lateral jets of water generated upon raindrop impact (Al-Durrah and Bradford 1982). Jets that are more horizontal will affect a larger radius around the point of raindrop impact, potentially accounting for the observed microcrater widening. This sequence of events may have been particularly efficient in the cases of MER and SC, which both rapidly developed a thin layer of closely packed fine ash particles near the surface hit by raindrops and showed signs of water saturation (but not ponding) near the surface during the simulated rainfall.

Evidence for surface crusting of the ash deposit

Ash particle cementation by mineral precipitates has been invoked to explain the presence of a crust at the surface of an ash deposit (Waldron 1967; Malin et al. 1983). Owing to its extremely high concentrations of dissolved calcium and sulphate (Table S2), SC ash was the most likely candidate for precipitation of an efficient cementing agent such as calcium sulphate (i.e. gypsum and possibly anhydrite). However, chemical cementation was not confirmed by SEM observations. This is probably due to rapid leaching of the soluble ions released from ash through the deposit and the underlying sand layer. Based on this result, we exclude salt precipitation as a main crust formation mechanism in our experiments.

In soil science, structural crusts are known to form at the soil surface in the absence of runoff (Valentin and Bresson 1992). Since in our experiments ponding did not occur and the deposit surfaces were kept horizontal, lateral redistribution and deposition of particles by runoff can be discarded as a potential crust formation mechanism. Thus, structural crusts formed on soils (Mualem et al. 1990; Valentin and Bresson 1992) represent a convenient model for investigating surface crusting of an ash deposit. In our study, exposure of MER, SC

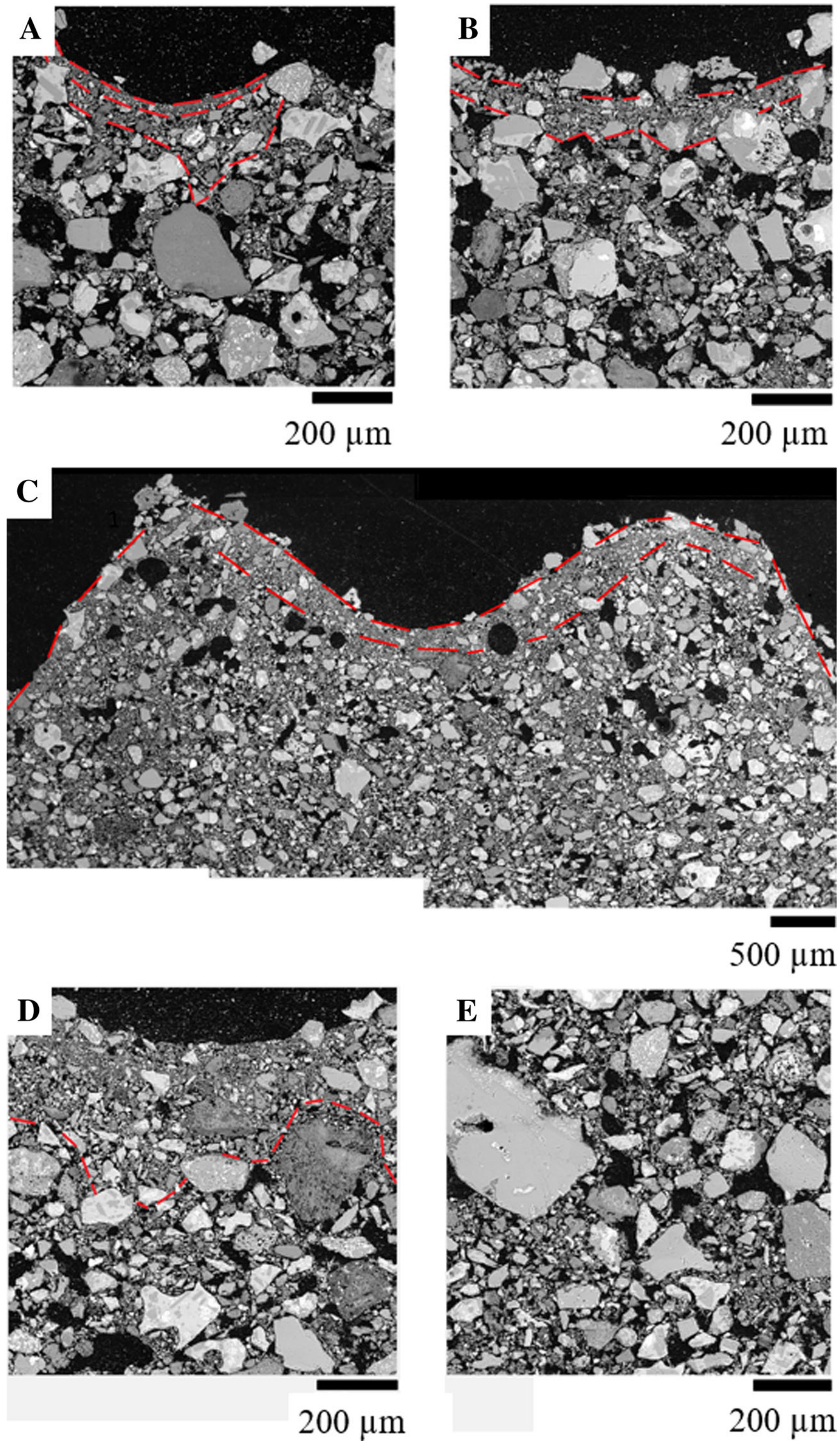

Fig. 6 SEM images of polished cross sections of the SC ash deposit after exposure to 5 (**a**), 10 (**b**) and 15 mm (**c** and **d**) of simulated rainfall. The red dashed lines delineate the near-surface layer in microcraters (**a**), (**b**) and (**d**), and in microcraters and on micropeaks (**c**) where particle reorganisation took place. The bulk material under this layer was unaffected by raindrop impact (**e**)

and EYJA ash deposits to direct raindrop impact clearly led to particle reorganisation near the deposit surface (Figs. 3, 4, 5, 6, 7 and 8). Particle reorganisation was a dynamic process as it rapidly evolved with continued rainfall. The most conspicuous changes were the appearance of microcraters and micropeaks shortly after initiation of rainfall, and the accumulation of micromass in the form of one or several layers a few tens to hundreds of micrometres thick. Such morphological features typically denote development of a structural crust (e.g. Mualem et al. 1990; Valentin and Bresson 1992; Bresson and Valentin 1993). Moreover, the tightly packed layer of fine particles found close to the surface of MER and SC displayed a systematic and significant reduction in porosity (Table S4).

Similar to what has been reported for coarse-textured soils or artificial mixtures dominated by sand fractions of various

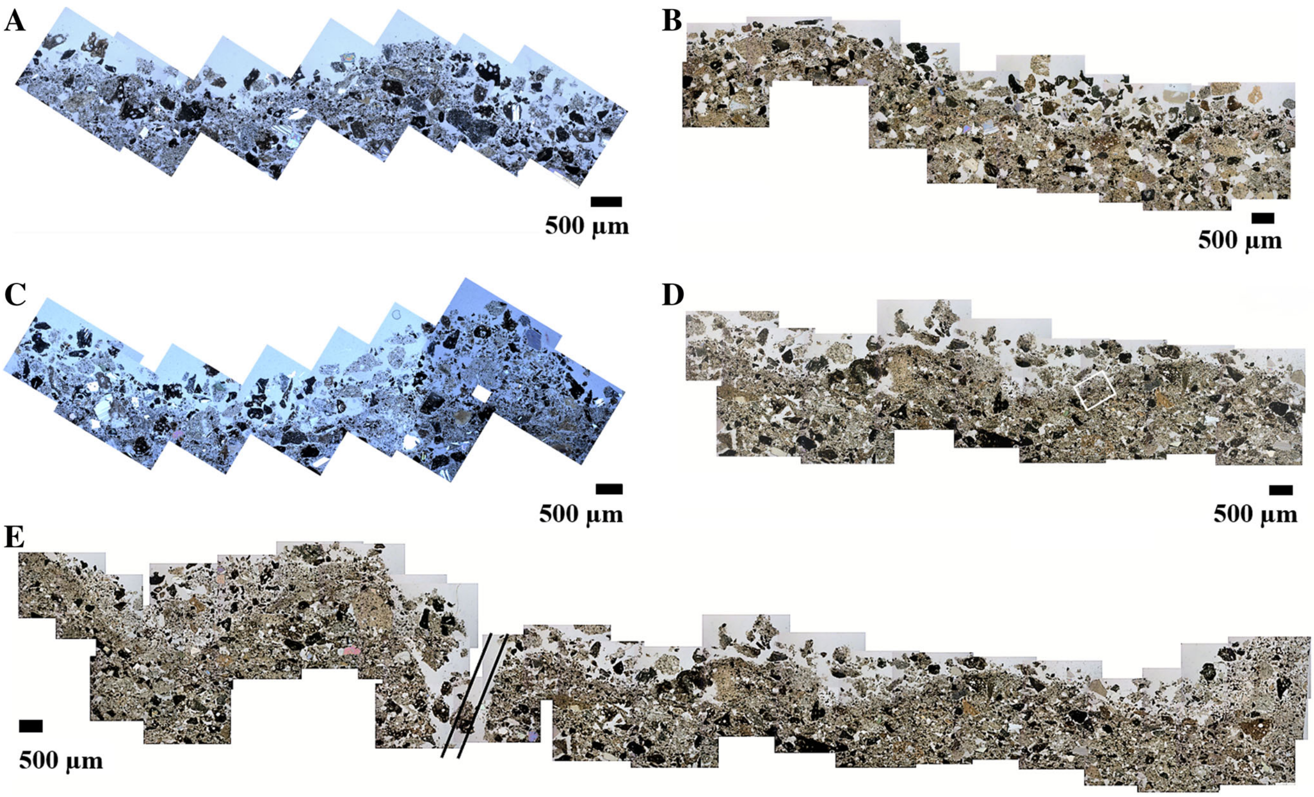

Fig. 7 Optical microscope images (stitched) of the thin cross sections of the EYJA ash deposit after exposure to 5 mm (**a**), 10 mm (**b**), 15 mm (**c**) and 20 mm (**d**) of rainfall. The rectangle outlined in white indicates the thin layer of tightly packed ash particles. The full cross section of the ash deposit surface exposed to 20 mm of simulated rain is shown in (**e**)

sizes (Valentin and Bresson 1992; Bielders and Baveye 1995a, b), we argue that crust formation at the surface of the ash deposit was strictly dependent upon the energy input from drop impact. Our results, which show that the ash deposits protected from direct raindrop impact did not exhibit any topographical or morphological modifications of their surfaces (Fig. S3), support this view. Consequently, the forces involved in wetting (i.e. physicochemical dispersion) and water infiltration (i.e. detachment by water shear stress and subsequent particle transport) alone were insufficient to induce surface crusting.

Mechanisms of crust formation in the ash deposit surface

Spatial differentiation of a structural crust in soils subjected to raindrop impact is the result of solid matter translocation (Valentin and Bresson 1992; Bresson and Valentin 1993). Comminution by wetting (i.e. slaking) and breakdown by raindrop impact of ash aggregates pre-existing in the artificial deposit may have contributed to ash crust formation. Although ash aggregates formed in volcanic plumes can be preserved in natural fallout deposits (Brown et al. 2012), we never observed these structures in our samples. It is also highly unlikely that, if present, ash aggregates would have survived the sample preparation step. We also posit that particle dispersion driven by physicochemical conditions did not play a significant role, as crusting was not observed on samples protected from raindrop impact. This most likely reflects the absence of particles with significant surface electrical charges in the ash deposits.

Four main mechanisms can potentially contribute to particle reorganisation during raindrop impact on non-aggregated material, such as the surface of our laboratory-reconstructed ash deposits. These include (i) compaction in response to the compressive stress generated during raindrop impact. The particle size distribution of the compacted layer remains identical to that of the original material, but the overall porosity is reduced (McIntyre 1958a, b; Epstein and Grant 1973); (ii) eluviation/illuviation as water penetrates into the ash deposit during drop impact, small particles may be entrained by hydraulic jets and the infiltrating water, leading to particle eluviation (Bresson and Valentin 1993; Hendrayanto et al. 1995). These particles may then accumulate again at some depth below the deposit surface (illuviation); (iii) particle sieving, i.e. the downward percolation of small particles in between coarser particles which results from the horizontal shear strain caused by raindrop impact (Bresson and Valentin 1993; Bielders and Baveye 1995a, b). The mechanism is applicable to granular media with limited cohesion between particles;

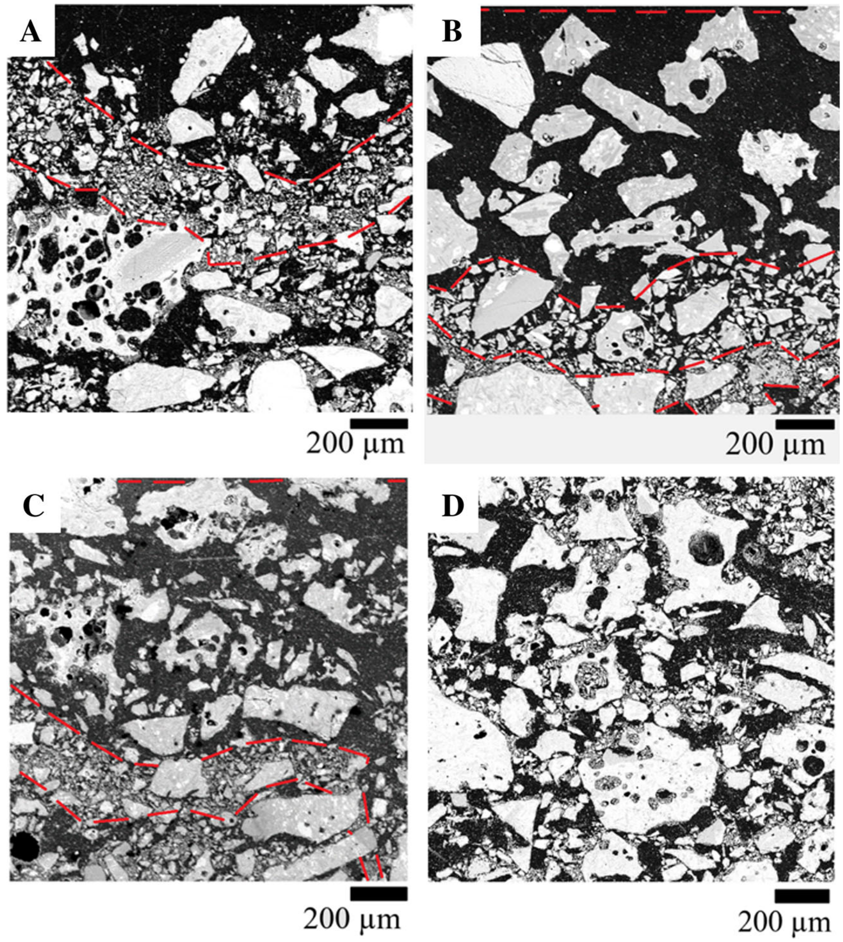

Fig. 8 SEM images of polished cross sections of the EYJA ash deposit after exposure to 5 (**a**), 10 (**b**) and 15 mm (**c**) of rainfall. The red dashed lines delineate the near-surface layer in microcraters (**a**), (**b**) and (**c**) where particle reorganisation took place. The bulk material under this layer was unaffected by raindrop impact (**d**)

(iv) splash, i.e. upon raindrop impact, droplets loaded with particles are ejected outwards, leading to lateral redistribution of material (Kinnell 2005). Mechanisms (i), (ii) and (iii) produce a vertical reorganisation of particles, whereas mechanism (iv) leads to horizontal particle redistribution. Contrary to compaction, (ii) and (iii) affect particle size distribution, with a relative enrichment in coarse particles near the surface (washed-out layer) and a relative enrichment in finer particles at some depth below the surface (washed-in layer).

MER ash deposit

A well-developed structural crust formed near the MER deposit surface (Figs. 3 and 4). As the experiment progressed, the crusts formed in microcraters and on micropeaks became more and more differentiated. From a morphological point of view, the crust associated with micropeaks evolved little with additional rainfall (Figs. 3 and 4, Table S3). In contrast, both the morphology and total thickness of the crust formed in microcraters changed significantly. Noticeably, a multi-layered crust developed in microcraters after 15 mm of rainfall (Figs. 3c–e and 4c). The generation of differentiated crusts implies that the surface microtopography remained reasonably stable after some time, despite raindrops hitting the surface randomly. In other words, microcraters that formed immediately after rainfall initiation acquired a stable position as the deposit surface wetted up and acquired a non-deformable behaviour. The increased mechanical strength of the surface as a result of wetting and/or structural crust formation may explain why the surface microtopography evolved towards a fairly stable configuration.

On micropeaks, the compressive stress resulting from raindrop impingement probably led to surface compaction and hence, decreased porosity (Table S4). In parallel, shear stress caused by hydraulic jets during raindrop impact led to splashing of particles outwards from the impact centre. Thus, raindrop impact can initiate a crust but can also partly disrupt it. While there were no direct signs of vertical particle segregation on micropeaks, washed-out coarse grains from the micropeaks may have been trapped in microcraters after being transported by splash, thereby contributing to the loose accumulation of coarse material on top of the thin layer of silt- and clay-size particles in micro-craters. In soils, vertical particle segregation is typically associated with coarse textures (Valentin and Bresson 1992; Bielders and Baveye 1995a). Thus, the absence of a washed-out layer in micropeaks may

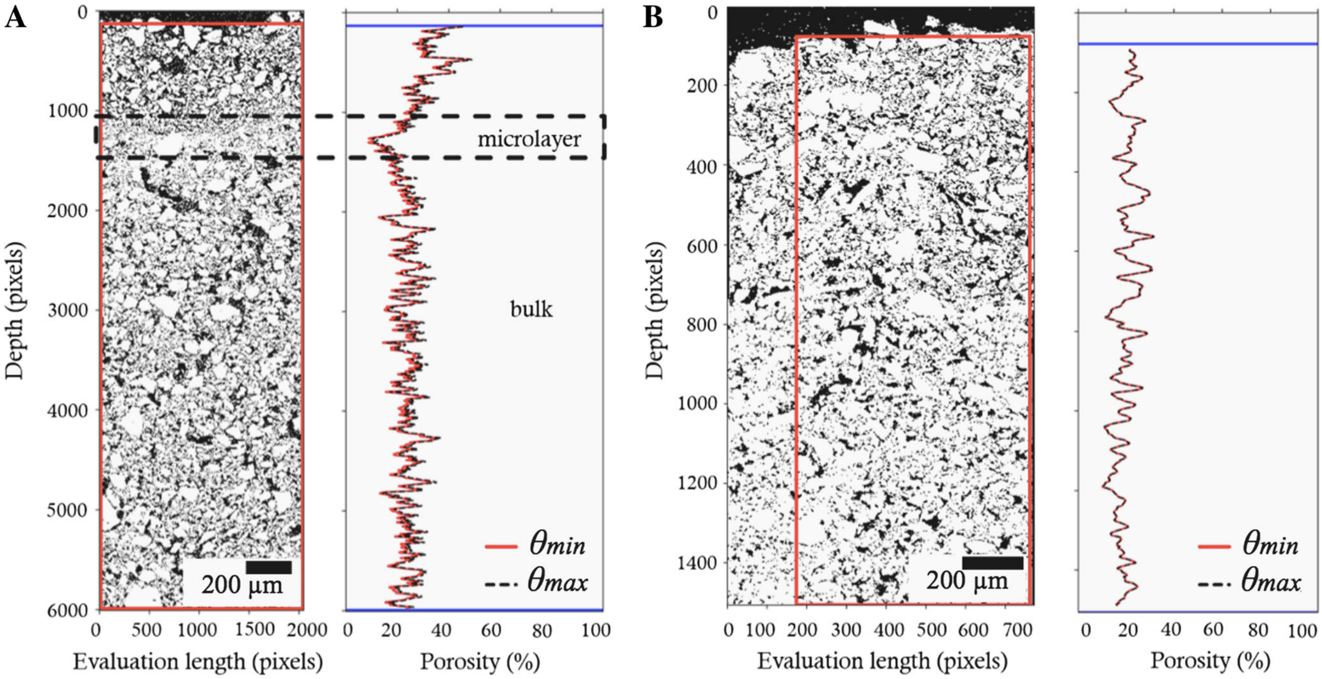

Fig. 9 Stitched images and corresponding porosity profiles of MER ash deposit after 10 mm of rainfall. Sample exposed to raindrop impact, 1 pixel = 0.48 µm × 0.48 µm (**a**); sample protected from raindrop impact, 1 pixel = 1.28 µm × 1.28 µm (**b**). The porosity profiles are plotted as 15-point moving averages. θ_{min} and θ_{max} correspond to the minimum and maximum percentage of pore area, respectively. The red rectangles in (**a**) and (**b**) indicate the areas used for calculations

relate to the relatively small content of coarse particles in MER ash (Fig. 2a, Table S1). Raindrops affected the whole deposit surface evenly and therefore, the initial stages of crust development in microcraters and on micropeaks were

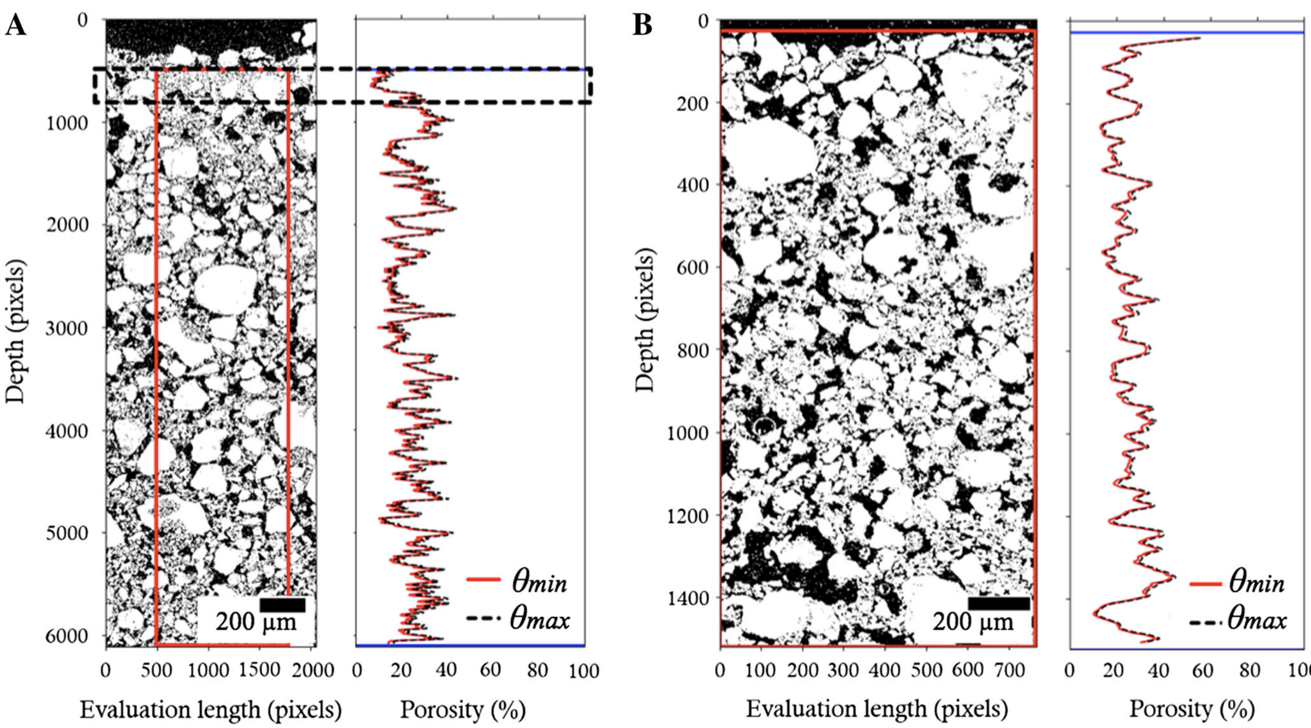

Fig. 10 Stitched images and corresponding porosity profiles of SC ash deposit after 10 mm of rainfall. Sample exposed to raindrop impact, 1 pixel = 0.48 µm × 0.48 µm (**a**); sample protected from raindrop impact, 1 pixel = 1.28 µm × 1.28 µm (**b**). The porosity profiles are plotted as 15-point moving averages. θ_{min} and θ_{max} correspond to the minimum and maximum percentage of pore area, respectively. The red rectangles in (**a**) and (**b**) indicate the areas used for calculations

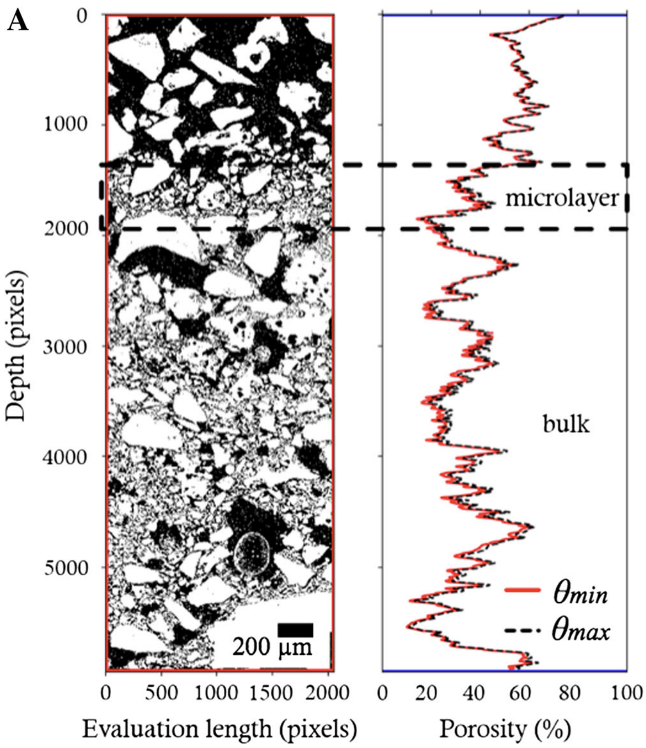

Fig. 11 Stitched images and corresponding porosity profiles of EYJA ash deposit after 10 mm of rainfall. Sample exposed to raindrop impact, 1 pixel = 0.70 µm × 0.70 µm (**a**); sample protected from raindrop impact, 1 pixel = 1.89 µm × 1.89 µm (**b**). The porosity profiles are plotted as 15-point moving averages. θ_{min} and θ_{max} correspond to the minimum and maximum percentage of pore area, respectively. Red rectangles in (**a**) and (**b**) indicate the areas used for calculations

probably governed by similar mechanisms. This is supported by a morphological resemblance between the thin layer of silt- and clay-size particles, which formed at the bottom of the microcraters and on micropeaks (Fig. 4a). For higher rainfall amounts, additional material enriched in coarser particles accumulated in microcraters, possibly due to preferential ejection of fine particles during splash (Moore and Singer 1990) and trapping of the splashed (coarser) material. As shown in Fig. 3b, vertical particle segregation affected the ash material amassed in microcraters. The vertical sorting of sand-size particles by raindrop impact is a phenomenon occurring in coarse-textured soils (e.g. Poss et al. 1990; Bielders and Baveye 1995a, b). It is likely the consequence of particle sieving and/or eluviation-illuviation. Since the depth affected by raindrop impact is relatively limited (Bielders and Baveye 1995a), the repeated accumulation of material and particle segregation led to smoothing of the deposit surface between 10 and 20 mm of rain (Fig. 2a) and to the development of multi-layered crusts near the MER surface, as observed after 15 and 20 mm of rain (e.g. Fig. 4c).

SC ash deposit

There were no clear signs of vertical particle segregation, neither on the micropeaks nor in the microcraters formed at the surface of SC deposit. Hence, crust formation after 5 mm of rainfall was probably driven mainly by compaction and splash. However, in contrast to MER, the thin layer of tightly packed fine particles was discontinuous (Figs. 5 and 6), possibly revealing a small shift in the balance between crust forming and crust destruction (by splash) mechanisms at the beginning of rainfall simulation. Such a shift may relate to the somewhat coarser texture of SC ash (Fig. 2b, Table S1) which would allow a deeper, and therefore more disruptive, impact of raindrop on the deposit surface (Bielders and Baveye 1995a).

In general, a coarse texture facilitates the downward movement of fine particles. However, vertical particle segregation occurred only occasionally in the SC ash deposit, despite a slightly coarser texture than the MER ash material (Fig. 2, Table S1). The latter is characterised by a more marked mode in the fine sand-coarse silt fraction (Fig. 2). It also exhibits a small secondary mode around 200 µm. In contrast, SC displays a rather homogeneous particle size distribution. The presence of strong modes in the particle size distribution of MER may have facilitated downward particle movement, and hence segregation, whereas the more homogeneous particle size distribution of SC ash may have impeded it.

Finally, rainfall amounts did not cause significant changes in SC crust features. In particular, multiple layering of coarse and fine material seldom took place in microcraters. This is reflected in the similar crust thicknesses in both microcraters and on micropeaks (Table S3).

EYJA ash deposit

Crusting of EYJA, the coarsest sample among the studied ash materials (Fig. 2c, Table S1), was erratic and less developed than for MER and SC. Washed-out coarse particles were apparent at all stages in microcraters, and often on micropeaks (Figs. 8a-c), forming a layer up to 1 mm thick after 20 mm of rainfall (Table S3). Despite the presence of a washed-out layer, micromass accumulation of tightly packed fine particles barely occurred in the EYJA deposit during the early stages of crust development. While this feature developed at higher rainfall amounts, it remained mostly discontinuous (Fig. 7). Similarly, Jones et al. (2017) noticed that rainfall did not lead to surface crust formation in ash dominated by coarse particles (D_{50} = 525.8 μm), although it did in a finer ash sample (D_{50} = 54.3 μm).

We postulate that the coarse ash texture, and resulting larger pore sizes and lower water content at all stages of the rainfall simulation, probably allowed water to penetrate easily into the deposit during raindrop impact. Thus, less energy was available for compaction, and this mechanism probably did not contribute significantly to crust formation.

The coarse texture, as well as the presence of a strong mode around 350 μm in the particle size distribution (Fig. 2c), should have favoured particle sieving and eluviation-illuviation as the main mechanisms leading to crust development in EYJA ash deposit. Hence, the comparatively slow rate of formation and discontinuous nature of the dense thin layer near the EYJA deposit surface is surprising. This could be an effect of ash particle shape; the ash material tended to be angular in EYJA whereas more round shapes characterised the MER and SC samples (e.g. Figs. 4, 6 and 8). Ash angularity may interfere with and impede the downward movement of small particles. It could also explain a lesser sensitivity to compaction.

Implications for natural ash deposits

Our laboratory experiments were limited to a single rainfall simulation on flat sample surfaces. In addition, we sought to avoid water ponding to characterise the first stage of structural crust development. However, under natural conditions, the surface of ash deposits may evolve in response to a range of factors and processes, including repeated rainfall events, duration and extent of ponding, particle translocation by wind erosion or overland flow, slope and particle redeposition. Rainfall events of longer duration or higher intensity may lead to water ponding at the surface of the deposit. This can affect the splash process or may cause runoff, thereby enhancing the risk of occurrence of lahars. Particle translocation by water erosion may lead to their sedimentation whenever the transport capacity of water decreases, e.g. at field edges or in depressions, resulting in the formation of sedimentary crusts (Bresson and Valentin 1993). Extended periods of desiccation between rainfall events may also take place, which was shown to create surface cracks, decrease surface runoff and increase infiltration of the ash deposits (Jones et al. 2017). Finally, raindrop size has been shown to partly dictate crust formation in soils (e.g. Epstein and Grant 1973; Bielders and Baveye 1995a, b). In our experiment, even though realistic rainfall kinetic energy values were achieved, a unique drop size was used. Under natural conditions, distribution of drop sizes exists, resulting in more impacts per unit area, and a wider range of drop kinetic energies, which may affect the intensity of the processes and hence the extent of the morphological changes observed in our study.

Conclusion

Exposure of three reconstructed ash deposits to simulated rainfall led to the formation of a structural crust near the deposit surface. The crust typically comprised a thin layer of tightly packed clay- and silt-size ash particles overlain by loose coarser materials, i.e. sieving structural crusts. The thin layer exhibited a lower porosity compared with bulk soil. We infer that crusting was governed primarily by ash particle reorganisation in response to raindrop impact, rather than by particle cementing through secondary salt precipitation. In the MER ash deposit, rain splash-driven particle detachment and compaction by raindrop impact initiated crust formation at the onset of rainfall. Sieving and eluviation/illuviation mechanisms became more important with additional rainfall, leading to vertical particle sorting and development of a multi-layered and thicker crust in micro-craters. In contrast to MER, particle sieving and eluviation/illuviation were subdued in SC ash, and crust formation was compaction dominated, i.e. packing structural crust. We interpret these contrasting behaviours as a consequence of different particle size distributions in MER and SC, the latter having a more uniform particle size distribution. In the case of EYJA, its coarse texture probably favoured rainwater percolation through the deposit and particle sieving and eluviation/illuviation. However, the crust remained discontinuous, possibly because of greater particle angularity.

Contrary to previous assumptions, our study does not support salt precipitation as a main crust formation mechanism (Waldron 1967). In any case, cementing of the ash surface due to salts is unlikely when the conditions (rainfall amount, ash hydraulic conductivity) allow for rapid leaching of soluble salts. Instead, we emphasise the important role of the particle size distribution of an ash fall deposit in dictating susceptibly to crusting. Ashfall deposits are usually size-sorted, and the finer material is typically transported and deposited farther away from the volcano. We show that a fine-grained material is more prone to surface crust formation upon raindrop impact and therefore, we may anticipate a differential impact with distance from the volcano, i.e. a distal, thin ash deposit could be more detrimental to soil-atmosphere exchanges than a proximal, thicker ash deposit. Moreover, since aggregate slaking during raindrop impact is recognised as an important component of physical crust formation in soil (e.g. Mualem et al. 1990; Valentin and Bresson 1992; Armenise et al. 2018), the presence of ash aggregates in a deposit will likely promote surface crusting.

Overall, our study provides novel insights for interpreting post-deposition crusting of a natural ash deposit. We presented benchmark experimental data on ash crust formation and concomitant reduction in porosity, which can also aid in the understanding of the factors controlling the initiation of rainfall-triggered lahars (Jones et al. 2017). Future experiments similar to those designed and developed here could encompass a broader range of ash types and rainfall parameters (for example, wetting-drying cycles) as well as rainfall simulations under field conditions allowing for particle redistribution by overland flow. This would further deepen our knowledge of the residence time of volcanic ash on the soil.

Acknowledgements We thank the Departamento de Metalurgia Extractiva, Escuela Politécnica Nacional, Quito, for access to their scanning electron microscope facility. The authors are grateful to an anonymous reviewer and to V. Manville, whose detailed and constructive comments greatly improved the quality of the manuscript. The authors would also like to thank the Associate Editor for his careful and swift handling of this contribution.

Funding information This study was supported by the Marie Curie Initial Training Network "VERTIGO" funded through the European Seventh Framework Program (FP7 2007-13) under Grant Agreement number 607905. I.T. benefited from a UCLouvain complementary PhD studentship (2017-18) funded through the Fonds Spéciaux de Recherche (FSR).

References

Al-Durrah MM, Bradford JM (1982) The mechanism of raindrop splash on soil surfaces 1. Soil Sci Soc Am J 46:1086–1090

Antos JA, Zobel DB (2005) Plant responses in forests of the tephra-fall zone. In: Dale VH, Swanson FJ, Crisafulli CM (eds) Ecological responses to the 1980 eruption of Mount St. Helens. Springer, New York, pp 47–58

Armenise E, Simmons RW, Ahn S, Garbout A, Doerr SH, Mooney SJ, Sturrock CJ, Ritz K (2018) Soil seal development under simulated rainfall: structural, physical and hydrological dynamics. J Hydrol 556:211–219

Arnalds O (2013) The influence of volcanic tephra (ash) on ecosystems. Adv Agron 121:331–380

Assouline S (2004) Rainfall-induced soil surface sealing. Vadose Zone J 3:570–591

Ayris PM, Delmelle P (2012) The immediate environmental effects of tephra emission. Bull Volcanol 74:1905–1936

Baumhardt RL, Schwartz RC (2004) Crusts. In: Hillel D (ed) Encyclopedia of soils in the environment. Elsevier Press, Oxford, pp 347–356

Bielders C, Baveye P (1995a) Processes of structural crust formation on coarse-textured soils. Eur J Soil Sci 46:221–232

Bielders C, Baveye P (1995b) Vertical particle segregation in structural crusts: experimental observations and the role of shear strain. Geoderma 67:247–261

Bielders C, Grymonprez B (2010) Raindrop impact: a neglected but potentially major contributor to particle mobilization in soils. Soil Sci Soc Am J 74:1446–1456

Black RA, Mack RN (1986) Mount St. Helens ash: recreating its effects on the steppe environment and ecophysiology. Ecology 67:1289–1302

Bresson LM, Valentin C (1993) Soil surface crust formation: contribution of micromorphology. Dev Soil Sci 22:737–762

Brown RJ, Bonadonna C, Durant AJ (2012) A review of volcanic ash aggregation. Phys Chem Earth A/B/C 45:65–78

Cook RJ, Barron JC, Papendick RI, Williams GJ (1981) Impact on agriculture of the Mount St. Helens eruptions. Science 211(4477):16–22

Craig H, Wilson T, Stewart C, Villarosa G, Outes V, Cronin S, Jenkins S (2016) Agricultural impact assessment and management after three widespread tephra falls in Patagonia, South America. Nat Hazards 82:1167–1229

Dale VH, Swanson FJ, Crisafulli CM (2005) Disturbance, survival, and succession: understanding ecological responses to the 1980 eruption of Mount St. Helens. In: Dale VH, Swanson FJ, Crisafulli CM (eds) Ecological responses to the 1980 eruption of Mount St Helens. Springer, New York, pp 3–11

Damby DE, Horwell CJ, Baxter PJ, Delmelle P, Donaldson K, Dunster C, Fubini B, Murphy FA, Nattrass C, Sweeney S, Tetley TD, Tomatis M (2013) The respiratory health hazard of tephra from the 2010 centennial eruption of Merapi with implications for occupational mining of deposits. J Volcanol Geotherm Res 261:376–387

Delmelle P, Villiéras F, Pelletier M (2005) Surface area, porosity and water adsorption properties of fine volcanic ash particles. Bull Volcanol 67:160–169

Epstein E, Grant WJ (1973) Soil crust formation as affected by raindrop impact. In: Hadas A, Swartzendruber D, Rijtema PE, Fuchs M, Yaron B (eds) Physical aspects of soil water and salts in ecosystems. Springer, Berlin, Heidelberg, Ecological Studies 4, pp 195–201

Global Volcanism Program (2000) Report on San Cristobal (Nicaragua). In: Wunderman R (ed.), Bulletin of the Global Volcanism Network. Smithsonian Institution, 25:2. http://www.volcano.si.edu/. Accessed 11 May 2018

Gudmundsson MT, Thordarson T, Höskuldsson Á et al (2012) Ash generation and distribution from the April-May 2010 eruption of Eyjafjallajökull, Iceland. Sci Rep 2:572

Hendrayanto KS, Takahisa M, Kosugi K (1995) Hydraulic characteristics of new volcanic ash deposit. J Jpn Soc Hydrol Water Res 8:484–491

Jones MT, Sparks RSJ, Valdes PJ (2007) The climatic impact of supervolcanic ash blankets. Clim Dyn 29:553–564

Jones R, Thomas RE, Peakall J, Manville V (2017) Rainfall runoff properties of tephra: simulated effects of grain-size and antecedent rainfall. Geomorphology 282:39–51

Kinnell PIA (2005) Raindrop-impact-induced erosion processes and prediction: a review. Hydrol Process 19:2815–2844

Leavesley GH, Lusby GC, Lichty RW (1989) Infiltration and erosion characteristics of selected tephra deposits from the 1980 eruption of Mount St. Helens, Washington, USA. Hydrol Sci J 34:339–353

Li Z, Giese RF, Wu W, Sheridan MF, Van Oss CJ (1997) The surface thermodynamic properties of some volcanic ash colloids. J Dispers Sci Technol 18:223–241

Malin MC, Dzurisin D, Sharp RP (1983) Stripping of Keanakakoi tephra on Kilauea volcano, Hawaii. GSA Bull 94:1148–1158

Manville V, Hodgson KA, Houghton BF, Keys JRH, White JDL (2000) Tephra, snow and water: complex sedimentary responses at an active snow-capped stratovolcano, Ruapehu, New Zealand. Bull Volcanol 62:278–293

McHale G, Newton MI, Shirtcliffe NJ (2005) Water repellent soil and its relationship to granularity, surface roughness and hydrophobicity: a materials science view. Eur J Soil Sci 56:445–452

McIntyre DS (1958a) Permeability measurements of soil crusts formed by raindrop impact. Soil Sci 85:185–189

McIntyre DS (1958b) Soil splash and the formation of surface crusts by raindrop impact. Soil Sci 85:261–266

Moore DC, Singer MJ (1990) Crust formation effects on soil erosion processes. Soil Sci Soc Am J 54:1117–1123

Moss AJ (1991) Rain impact soil crust. I. Formation on a granite derived soil. Soil Res 29:271–289

Mualem Y, Assouline S, Rohdenburg H (1990) Rainfall induced soil seal. (A) a critical review of observations and models. Catena 17:185–203

Nammah H, Larsen FE, McCool DK, Fritts R, Molnau M (1986) Mt. St. Helens volcanic ash: effect of incorporated and unincorporated ash of two particle sizes on runoff and erosion. Agric Ecosyst Environ 15:63–72

Pierson TC, Major JJ (2014) Hydrogeomorphic effects of explosive volcanic eruptions on drainage basins. Annu Rev Earth Planet Sci 42: 469–507

Poss R, Pleuvret C, Saragoni H (1990) Influence des réorganisations superficielles sur l'infiltration dans les terres de Barre (Togo méridional). Cahiers-ORSTOM Pédologie 25:405–415

Segerstrom K (1950) Erosion studies at Paricutin, state of Michoacan, Mexico. Report, USGS Numbered Series, Bulletin 965-A, pp 1–164

Sigmarsson O, Vlastelic I, Andreasen R, Bindeman I, Devidal JL, Moune S, Keiding JK, Larsen G, Höskuldsson A, Thordarson T (2011) Remobilization of silicic intrusion by mafic magmas during the 2010 Eyjafjallajökull eruption. Solid Earth 2:271–281

Valentin C, Bresson LM (1992) Morphology, genesis and classification of surface crusts in loamy and sandy soils. Geoderma 55:225–245

Waldron HH (1967) Debris flow and erosion control problems caused by the ash eruptions of Irazu volcano, Costa Rica. US Geol Surv Bull 1241:1–37

Yamakoshi T, Suwa H (2000) Post-eruption characteristics of surface runoff and sediment discharge on the slopes of pyroclastic flow deposits, Mount Unzen, Japan. Trans Jpn Geomorphol Union 21: 469–497